

Theoretical study on the crystal structure of a bilayer nickel-oxychloride $\text{Sr}_3\text{Ni}_2\text{O}_5\text{Cl}_2$ and analysis on the occurrence of possible unconventional superconductivity

Masayuki Ochi,^{1,2,*} Hirofumi Sakakibara,^{3,*} Hidetomo Usui,⁴ and Kazuhiko Kuroki^{2,†}

¹*Forefront Research Center, Osaka University, 1-1 Machikaneyama-cho, Toyonaka, Osaka 560-0043, Japan*

²*Department of Physics, Osaka University, 1-1 Machikaneyama-cho, Toyonaka, Osaka 560-0043, Japan*

³*Advanced Mechanical and Electronic System Research Center (AMES),*

Faculty of Engineering, Tottori University, 4-10 Koyama-cho, Tottori, Tottori 680-8552, Japan

⁴*Department of Applied Physics, Shimane University,*

1060 Nishikawatsu-cho, Matsue, Shimane 690-8504, Japan

(Dated: December 30, 2024)

The discovery of superconductivity under high pressure with T_c exceeding 80 K in a bilayer nickelate $\text{La}_3\text{Ni}_2\text{O}_7$ has led to a strong desire to realize similar high T_c phenomena at ambient pressure. As one possible path toward realizing superconductivity at ambient pressure, we here propose to consider $\text{Sr}_3\text{Ni}_2\text{O}_5\text{Cl}_2$ as a possible candidate. In this study, we theoretically investigate the electronic structure of $\text{Sr}_3\text{Ni}_2\text{O}_5\text{Cl}_2$ and its structural stability. Our phonon calculation shows that this compound with the $I4/mmm$ tetragonal structure is dynamically stable even at ambient pressure. The characteristic crystal field in this compound lowers the Ni- $d_{3z^2-r^2}$ orbital energy, by which the Ni- $d_{3z^2-r^2}$ orbital becomes rather closer to the half-filling in $\text{Sr}_3\text{Ni}_2\text{O}_5\text{Cl}_2$ than $\text{La}_3\text{Ni}_2\text{O}_7$. As a result, we find that superconductivity is enhanced even though a relatively strong orbital hybridization between the t_{2g} and e_g orbitals is somewhat detrimental for superconductivity. We also check the formation enthalpy, which shows that the high-pressure synthesis can be a good way to actually produce $\text{Sr}_3\text{Ni}_2\text{O}_5\text{Cl}_2$. We find that $\text{Sr}_3\text{Ni}_2\text{O}_5\text{Cl}_2$ is a promising new candidate of bilayer-nickelate superconductors, which can possess even higher T_c than pressurized $\text{La}_3\text{Ni}_2\text{O}_7$, at ambient pressure.

I. INTRODUCTION

Discovery of superconductivity with a maximum T_c of above 80 K in a bilayer Ruddlesden-Popper nickelate $\text{La}_3\text{Ni}_2\text{O}_7$ (Fig. 1(a)) under pressure has sparked enormous interest in the field of condensed matter physics [1]. Although under pressure, T_c exceeding the liquid nitrogen boiling temperature, and also the origin of superconductivity likely being unconventional [2–4], have led to a huge amount of experimental and theoretical studies after the discovery [1–77]. In fact, the possibility of superconductivity in this material was discussed theoretically even before its experimental discovery by some of the previous authors [78], but one viewpoint that was missing at that time was the precise crystal structure, namely, although a tetragonal symmetry was simply assumed in Ref. 78, the actual structural symmetry is orthorhombic at ambient pressure. There are now accumulating studies suggesting that tetragonal symmetry of the crystal structure may be important for the occurrence of superconductivity in $\text{La}_3\text{Ni}_2\text{O}_7$ [32, 41, 42], which is accomplished by applying pressure. One speculation regarding the reason for this can be that orthorhombicity favors density waves, which suppresses superconductivity. Interestingly, also for the trilayer compound $\text{La}_4\text{Ni}_3\text{O}_{10}$, the superconducting phase appears by applying a sufficient pressure and the tetragonal structure is realized [31, 38–40, 48]. Then, a natural motivation arises for searching materials that

have tetragonal symmetry at ambient pressure, and also have electronic properties similar to that of $\text{La}_3\text{Ni}_2\text{O}_7$ at high pressures.

One path toward realizing tetragonal symmetry at ambient pressure is to replace the rare earth (La) atom with an element with larger ion radius, which however is not possible within lanthanoids since La has the largest ion radius [25, 32]. Hence, there is a proposal for using actinium instead [33, 69], which however is strongly radioactive. Alkaline-earth elements such as Sr and Ba [33] have larger ion radius than La, but the valence is 2+ rather than 3+, which results in a nickel valence of 4+, which is not typical. These considerations have led us to consider the possibility of $\text{Sr}_3\text{Ni}_2\text{O}_5\text{Cl}_2$ (Fig. 1(b)) as a possible candidate for our purpose, where the two chlorines replace the outer apical oxygens to reduce the nickel valence. The nickel valence is 3+ as compared to 2.5+ in $\text{La}_3\text{Ni}_2\text{O}_7$, but an expectation is that the $d_{3z^2-r^2}$ band filling, which has been shown to be crucial for superconductivity in $\text{La}_3\text{Ni}_2\text{O}_7$, could be similar because the energy level offset ΔE between $d_{3z^2-r^2}$ and $d_{x^2-y^2}$ is expected to be larger in $\text{Sr}_3\text{Ni}_2\text{O}_5\text{Cl}_2$ due to the outer apical oxygens being replaced by chlorine. Although this material has not been synthesized to our knowledge, its iron and cobalt analogues $\text{Sr}_3\text{Fe}_2\text{O}_5\text{Cl}_2$ [79] and $\text{Sr}_3\text{Co}_2\text{O}_5\text{Cl}_2$ [80] have been synthesized in the past, and the crystal structure is known to have tetragonal symmetry. It is noteworthy that oxychlorides have also been investigated in the study of cuprate superconductors such as $(\text{Ca},\text{Na})_2\text{CuO}_2\text{Cl}_2$ [81], where the crystal field of the transition metal atom and the carrier concentration are changed via anion substitution. Recently, another mixed-

* These authors contributed equally to this work.

† kuroki@phys.sci.osaka-u.ac.jp

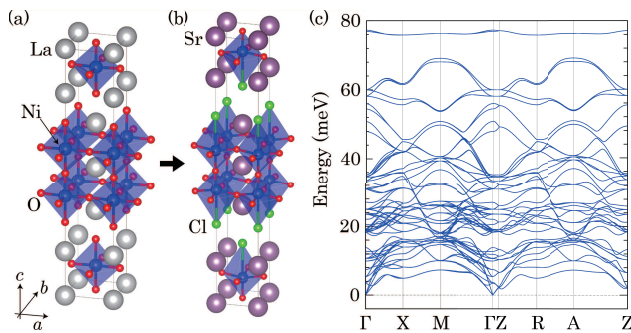


FIG. 1. (a) Crystal structure of $\text{La}_3\text{Ni}_2\text{O}_7$ at high pressure. (b) Crystal structure and (c) phonon band dispersion for $\text{Sr}_3\text{Ni}_2\text{O}_5\text{Cl}_2$ without applying pressure. Panels (b) and (c) are shown for the space group of $I4/mmm$. Crystal structures in this paper were depicted using the VESTA software [82]. Phonon dispersions in this paper were depicted in the Brillouin zone of the conventional tetragonal lattice.

anion nickelate $\text{La}_2\text{AeNi}_2\text{O}_6\text{F}$ has been proposed as a material having tetragonal symmetry at ambient ($\text{Ae} = \text{Ba}$) or low ($\text{Ae} = \text{Sr}$) pressure [69], but our proposal is different in that the inner apical oxygen, which we believe to be playing a crucial role in the occurrence of superconductivity in $\text{La}_3\text{Ni}_2\text{O}_7$ is maintained, while outer apical oxygens are replaced by halogens.

In this study, we theoretically investigate the electronic structure of $\text{Sr}_3\text{Ni}_2\text{O}_5\text{Cl}_2$ and its structural stability. Our phonon calculation shows that this compound with the $I4/mmm$ tetragonal structure is dynamically stable, i.e., does not have imaginary-frequency phonon modes, even at ambient pressure. The $\text{Ni}-d_{3z^2-r^2}$ orbital energy is pushed down by the crystal field where half of the apical O^{2-} ions are replaced with a Cl^- ion. By this effect, the $\text{Ni}-d_{3z^2-r^2}$ orbital becomes rather closer to the half-filling in $\text{Sr}_3\text{Ni}_2\text{O}_5\text{Cl}_2$ than $\text{La}_3\text{Ni}_2\text{O}_7$ whereas the stoichiometric $\text{Ni}-3d$ band filling are decreased in $\text{Sr}_3\text{Ni}_2\text{O}_5\text{Cl}_2$ ($d^{7.5}$) compared with $\text{La}_3\text{Ni}_2\text{O}_7$ ($d^{7.5}$). We also investigate superconductivity in this compound with the multi-orbital Hubbard model constructed from our first-principles calculation, using the fluctuation exchange (FLEX) approximation combined with the linearized Eliashberg equation. While orbital hybridization between the t_{2g} and e_g orbitals, which is enhanced in this characteristic crystal field, is detrimental for superconductivity, a nearly half-filled $\text{Ni}-d_{3z^2-r^2}$ orbital enhances superconductivity. In total, we find that $\text{Sr}_3\text{Ni}_2\text{O}_5\text{Cl}_2$ is a promising new candidate of bilayer-nickelate superconductors, which can possess even higher T_c than pressurized $\text{La}_3\text{Ni}_2\text{O}_7$, at ambient pressure. We also check the formation enthalpy for synthesis of this compound. Our calculation shows that the high-pressure synthesis can be a good way to experimentally produce $\text{Sr}_3\text{Ni}_2\text{O}_5\text{Cl}_2$.

II. METHODS

For first-principles calculation, we used the PBEsol exchange-correlation functional [83] and the projector augmented wave method as implemented in *Vienna ab initio Simulation Package* (VASP) [84–88]. Core-electron states in PAW potentials were $[\text{Kr}]4d^{10}$, $[\text{Ar}]3d^{10}$, $[\text{Ar}]$, $[\text{Ne}]$, and $[\text{He}]$ for La, Sr, Ni, Cl, and O, respectively. We used a plane-wave cutoff energy of 600 eV for Kohn-Sham orbitals without including the spin-orbit coupling for simplicity. A $12 \times 12 \times 12$ \mathbf{k} -mesh was used for self-consistent-field calculations.

We performed structural optimization until the Hellmann-Feynman force becomes less than $0.01 \text{ eV } \text{\AA}^{-1}$ for each atom. To check the stability of the tetragonal ($I4/mmm$) phase, we calculated the phonon dispersion for several materials. For this purpose, we used the finite displacement method as implemented in the PHONOPY [89, 90] software in combination with VASP. We used a $4 \times 4 \times 1$ \mathbf{q} -mesh for a conventional tetragonal unit cell. For a $4 \times 4 \times 1$ supercell used for finite-displacement calculations, we used a $3 \times 3 \times 2$ \mathbf{k} -mesh.

To discuss superconductivity, we constructed a model Hamiltonian of $\text{Ni}-3d$ orbitals in the following way. We extracted five $3d$ -like Wannier orbitals per Ni site using WANNIER90 software [91–93]. For this purpose, we used a $12 \times 12 \times 12$ \mathbf{k} -mesh for a primitive unit cell. We constructed a model Hamiltonian by adding the on-site interaction terms to the tight-binding Hamiltonian obtained through Wannierization. We took the on-site interactions, namely, intraorbital (interorbital) Coulomb interactions U (U'), Hund's coupling J , and pair hopping J' . We assumed the orbital-rotational symmetry, namely, we took the same value of U for all $3d$ orbitals preserving the equations $U' = U - 2J$ and $J = J'$. We took $U = 3 \text{ eV}$, $J = J' = U/10 = 0.3 \text{ eV}$ and $U' = U - 2J = 2.4 \text{ eV}$, which can be considered as typical values for $3d$ -transition-metal oxides.

We adopted FLEX [94, 95] to analyze electron correlation effects for the Hubbard model as was done in Ref. [8]. We calculated the self-energy induced by the spin-fluctuation formulated as shown in the literatures [96–98] in a self-consistent calculation. The real part of the self-energy at the lowest Matsubara frequency was subtracted in the same manner as Ref. [99] to maintain the band structure around the Fermi level obtained by first-principles calculation. We used the linearized Eliashberg equation to study the possibility of superconductivity in $\text{Sr}_3\text{Ni}_2\text{O}_5\text{Cl}_2$ comparing with $\text{La}_3\text{Ni}_2\text{O}_7$. The renormalized Green's functions obtained by FLEX were plugged into this equation. Note that the pairing interaction kernel in this equation was obtained from the FLEX Green's function as a purely electronic one (i.e. phonon-mediated pairing interaction was not considered), which is mainly dominated by spin fluctuations in the present case. Since the eigenvalue λ of the Eliashberg equation monotonically increases upon lowering the temperature T , and reaches unity at $T = T_c$, we adopted λ calculated

at a fixed temperature, $T = 0.01$ eV, as a measure of superconductivity. For convenience, we will call the eigenfunction (with the largest eigenvalue) of the linearized Eliashberg equation at the lowest Matsubara frequency $i\omega = i\pi k_B T$ the “superconducting gap function”. We took a $16 \times 16 \times 4$ \mathbf{k} -mesh and 2048 Matsubara frequencies for the FLEX calculation.

For calculating the formation energy, we adopted space groups taken from experimental studies: $Fm\bar{3}m$ for SrO, SrCl₂, Ni, NiO, $I4/mmm$ for SrCl₂, Sr₂NiO₂Cl₂ [100], $Cmcm$ for SrNiO₂ [101], and $P6_3/mmc$ for SrNiO₃ [102]. An isolated O₂ molecule was calculated in a $15 \text{ \AA} \times 15 \text{ \AA} \times 15 \text{ \AA}$ cell considering the spin-triplet ground state with the spin-polarized calculation.

III. RESULTS AND DISCUSSIONS

A. Electronic and phonon band structures for Sr₃Ni₂O₅Cl₂

As described in the Introduction, a key idea in this study is to employ a mixed-anion strategy [103] for stabilizing the tetragonal $I4/mmm$ phase without applying the pressure. In fact, for Sr₃Ni₂O₅Cl₂, while the NiO₂ plane is somewhat buckled; the equatorial Ni-O-Ni angle is 162° as shown in Fig. 1(b), we found that the tetragonal structure ($a = 3.779 \text{ \AA}$, $c = 24.532 \text{ \AA}$) is dynamically stable as shown by our phonon calculation (Fig. 1(c)) where no imaginary-frequency modes appear without applying the pressure. This is in sharp contrast to the case of La₃Ni₂O₇, where the tetragonal structure is unstable at ambient pressure and high pressure is required to stabilize it [32, 41, 42]. Our phonon calculations for La₃Ni₂O₇ also support this feature as shown in Fig. 6, where the imaginary-frequency modes appear for 0 GPa while they are absent for 20 GPa. Although we also checked the stability of the tetragonal structure for Sr₃Ni₂O₄Cl₃, where all the apical oxygens were replaced with chlorines, we found that the tetragonal structure was unstable for this case as shown in Fig. 7. We consider that one important difference among these compounds is the average valence number of the nickel atom: Ni^{2.5+} ($d^{7.5}$) for La₃Ni₂O₇ and Sr₃Ni₂O₄Cl₃ while Ni³⁺ (d^7) for Sr₃Ni₂O₅Cl₂. Here, the size of the nickel ion becomes smaller in Sr₃Ni₂O₅Cl₂, which in general suppresses the rotational and tilting instability of octahedra in Ruddlesden-Popper phase materials.

It is noteworthy that the mixed-anion strategy drastically changes the crystal field of a nickel ion. Figure 2 presents the electronic band structures and partial density of states (pDOS) for La₃Ni₂O₇ under pressure of 20 GPa and Sr₃Ni₂O₅Cl₂ without applying the pressure shown with an orbital weight of each Ni- d orbital. We summarize important differences between two materials from the viewpoint of the crystal field as follows.

As mentioned above, the average valence number of the nickel atom is different: Ni^{2.5+} ($d^{7.5}$) for La₃Ni₂O₇

and Ni³⁺ (d^7) for Sr₃Ni₂O₅Cl₂. Thus, the number of d electrons for Sr₃Ni₂O₅Cl₂ is less than that for La₃Ni₂O₇. Nevertheless, the Ni- $d_{3z^2-r^2}$ orbital is rather closer to the half-filling in Sr₃Ni₂O₅Cl₂ as shown in Figs. 2(b)(h). This is because of the characteristic crystal field for the nickel atom in Sr₃Ni₂O₅Cl₂, where a half of apical O²⁻ ions is replaced with a Cl⁻ ion, which pushes down the orbital energy of the Ni- $d_{3z^2-r^2}$ orbital. As a result, the number of $d_{x^2-y^2}$ electrons is decreased in Sr₃Ni₂O₅Cl₂. On the other hand, Ni- $d_{xy/yz/zx}$ orbitals, which we hereafter call them the t_{2g} orbitals while it is not a rigorous term for this symmetry, raise their energy levels relative to the Ni- $d_{3z^2-r^2}$ orbital. This is because the present crystal field strongly pushes down the Ni- $d_{3z^2-r^2}$ orbital level as we have stated above. Consequently, the strong DOS peak of the t_{2g} orbitals lies just below the Fermi energy. In addition, the crystal field is strongly asymmetric with respect to the xy plane (i.e., $+z$ and $-z$ are strongly inequivalent), which allows a sizable hybridization among e_g ($d_{x^2-y^2}$ and $d_{3z^2-r^2}$) and t_{2g} orbitals. In the next section, we will discuss how these characteristics can affect superconductivity in this system.

B. Model construction

In this and the next sections, we compared Sr₃Ni₂O₅Cl₂ without applying the pressure and La₃Ni₂O₇ under pressure of 20 GPa, both of which have the $I4/mmm$ tetragonal structure in our calculation. We constructed a ten-orbital model consisting of five $3d$ orbitals centered at two Ni sites per unit cell. Figure 3(a) shows superposed band structures given by first-principles calculation and Wannier interpolation, where precise fitting around the Fermi level was achieved. Important parameter values extracted by Wannierization are given in Table I, compared with those of four-orbital models consisting only of e_g orbitals. The smaller differences in extracted parameters between the ten- and four-orbital models for La₃Ni₂O₇ originate from the fact that the e_g and t_{2g} bands are well separated compared with Sr₃Ni₂O₅Cl₂, where the t_{2g} and e_g bands are rather entangled, as shown in Fig. 2. We found a relatively large hopping amplitude between t_{2g} and e_g orbitals: e.g., the nearest-neighbor intralayer hopping along the x direction between the $d_{x^2-y^2}$ and d_{xz} orbitals and that between the $d_{3z^2-r^2}$ and d_{xz} orbitals are -0.296 and 0.199 eV, respectively. This is due to the strongly asymmetric crystal field for a NiO₅Cl octahedron as mentioned in the previous section. It is also noteworthy that the relatively strong buckling of NiO₂ plane in Sr₃Ni₂O₅Cl₂ seems to enhance the vertical interlayer hopping t_\perp between the $d_{3z^2-r^2}$ orbitals while the nearest-neighbor intralayer hoppings $t_{3z^2-r^2}$, $t_{x^2-y^2}$, and $t_{x^2-y^2-3z^2-r^2}$ are somewhat suppressed as shown in Table I. For Sr₃Ni₂O₅Cl₂, we also found that the onsite energies of the d_{xy} and $d_{yz/zx}$ orbitals relative to that for the $d_{3z^2-r^2}$ orbital are -0.811 eV and -0.840

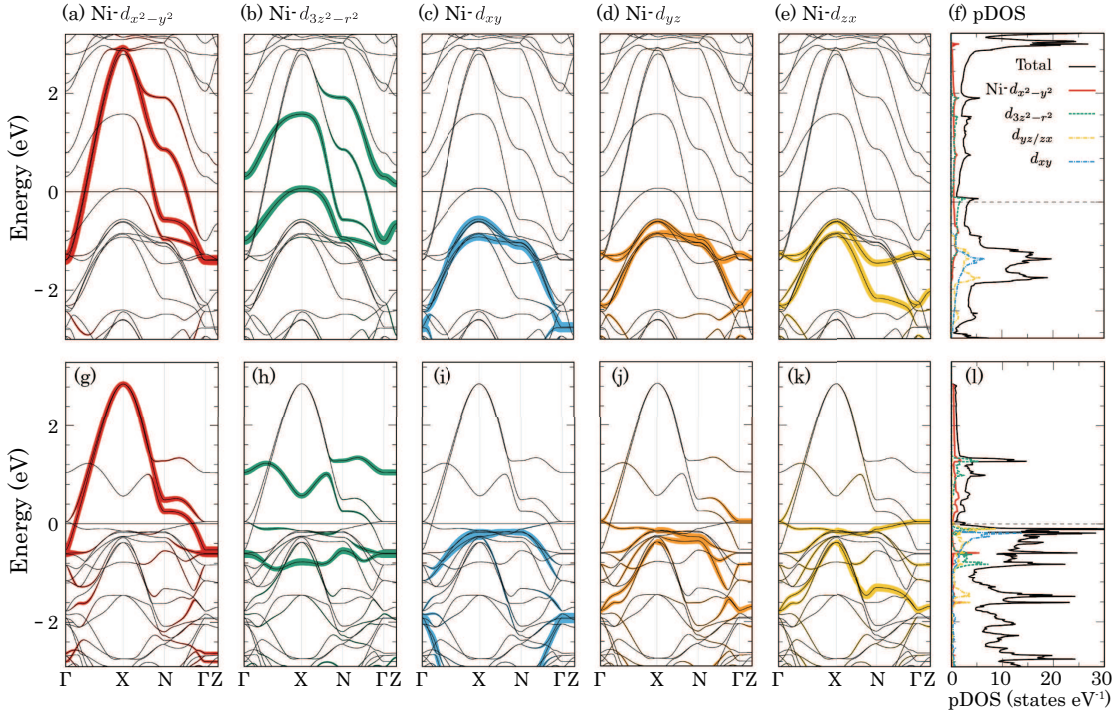


FIG. 2. Electronic band dispersion with a colored weight of Ni- (a) $d_{x^2-y^2}$, (b) $d_{3z^2-r^2}$, (c) d_{xy} , (d) d_{yz} , and (e) d_{zx} orbitals, respectively, and (f) pDOS for $\text{La}_3\text{Ni}_2\text{O}_7$ under pressure of 20 GPa. (g)–(l) Same plots for $\text{Sr}_3\text{Ni}_2\text{O}_5\text{Cl}_2$ without applying the pressure.

eV, respectively, the size of which are comparable to $\Delta E = E_{x^2-y^2} - E_{3z^2-r^2} = 0.776$ eV listed in Table I.

TABLE I. The orbital level offset $\Delta E = E_{x^2-y^2} - E_{3z^2-r^2}$ between the $d_{x^2-y^2}$ and the $d_{3z^2-r^2}$ orbitals, the vertical interlayer hopping t_{\perp} between the $d_{3z^2-r^2}$ orbitals, and the nearest-neighbor intralayer hoppings $t_{3z^2-r^2}$, $t_{x^2-y^2}$, and $t_{x^2-y^2-3z^2-r^2}$ are displayed. The first column indicates the chemical formulae of the calculated materials, where the number in the round brackets indicate the number of orbitals.

(eV)	ΔE	t_{\perp}	$t_{3z^2-r^2}$	$t_{x^2-y^2}$	$t_{x^2-y^2-3z^2-r^2}$
$\text{Sr}_3\text{Ni}_2\text{O}_5\text{Cl}_2$ (10)	0.776	-0.744	0.041	-0.425	-0.086
$\text{Sr}_3\text{Ni}_2\text{O}_5\text{Cl}_2$ (4)	0.920	-0.786	0.037	-0.383	-0.074
$\text{La}_3\text{Ni}_2\text{O}_7$ (10)	0.343	-0.660	-0.126	-0.499	-0.253
$\text{La}_3\text{Ni}_2\text{O}_7$ (4)	0.328	-0.659	-0.128	-0.501	-0.253

In Fig. 3(b), we plot the number of electrons for each orbital per Ni against the hypothetically varied total band filling, assuming a rigid band. In this paper, the total band filling n is defined as the number of electrons per spin in the primitive unit cell, e.g., $0 \leq n \leq 10$ for ten-orbital models. The doping ratio Δn is defined as the deviation of the total band filling from its value at stoichiometry. In $\text{Sr}_3\text{Ni}_2\text{O}_5\text{Cl}_2$, the number of electrons occupying the $d_{3z^2-r^2}$ band per Ni, called $n[d_{3z^2-r^2}]$ hereafter, exceeds unity (half-filled) already at stoichiometry, consistent with the observation given in Section III A. Also, the $d_{yz/zx}$ orbitals are not fully filled due to the hybridization with the e_g orbitals. Contrastingly, in $\text{La}_3\text{Ni}_2\text{O}_7$, the $d_{yz/zx}$ orbitals are fully filled in the whole doping range suggesting their irrelevance for supercon-

ductivity and justifying the previously proposed four-orbital model [8].

Based on the observation described in this section, we used the ten-orbital model for $\text{Sr}_3\text{Ni}_2\text{O}_5\text{Cl}_2$ and the four-orbital model (i.e., e_g model) for $\text{La}_3\text{Ni}_2\text{O}_7$ at 20 GPa in the following analysis of superconductivity.

C. FLEX analysis on superconductivity in $\text{Sr}_3\text{Ni}_2\text{O}_5\text{Cl}_2$

In the left panel of Fig. 3(c), we plot the eigenvalue λ of the linearized Eliashberg equation against Δn . For comparison, we also plot λ for models where (i) the $t_{2g} - e_g$ interorbital interactions are turned off, and (ii) all the interorbital interactions are turned off. λ is also plotted for the four-orbital model of $\text{La}_3\text{Ni}_2\text{O}_7$. By comparing λ calculated with the original (full) model and that calculated by the condition (i), it can be seen that the $t_{2g} - e_g$ interorbital interactions somewhat suppress superconductivity in $\text{Sr}_3\text{Ni}_2\text{O}_5\text{Cl}_2$. Still, quite interestingly, the value of λ of the full model of $\text{Sr}_3\text{Ni}_2\text{O}_5\text{Cl}_2$ is significantly larger than that of $\text{La}_3\text{Ni}_2\text{O}_7$ at stoichiometry, suggesting the possibility that the material possesses a potential of even higher T_c than 80 K *at ambient pressure*. Also, a slight electron doping may result in an even higher T_c . Electron doping is expected to be possible by partially substituting Sr by La, for which we have also verified the stability of the tetragonal symme-

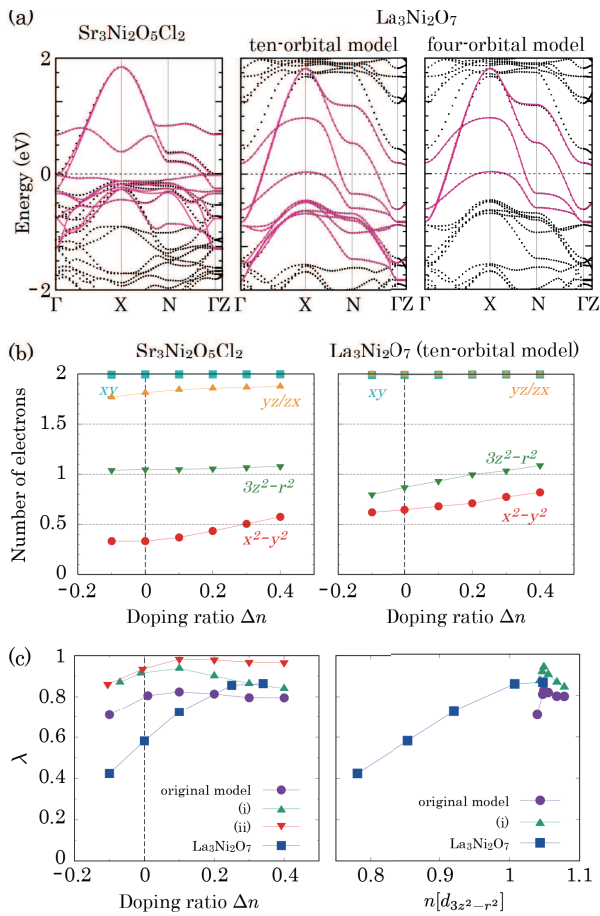


FIG. 3. (a) Band structure of the ten-orbital model (pink solid lines) superposed on that obtained from first-principles calculation (black dotted lines) for Sr₃Ni₂O₅Cl₂ (left) and those for the ten-orbital model (middle) and the four-orbital model (right) of La₃Ni₂O₇, (b) the number of electrons per Ni for each orbital as a function of doping ratio Δn for Sr₃Ni₂O₅Cl₂ (left) and La₃Ni₂O₇ (right), (c) the eigenvalue λ of the linearized Eliashberg equation at $T = 0.01$ eV as a function of Δn (left) and $n[d_{3z^2-r^2}]$ (right), where the case of stoichiometry is indicated by arrows. In panel (c), the legend (i) indicates the case that the $t_{2g} - e_g$ interorbital interactions are turned off, and (ii) all the interorbital interactions are turned off. The legend “La₃Ni₂O₇” in panel (c) indicates the result of four-orbital-model calculation.

try as shown in Fig. 8(b), where no imaginary-frequency phonon modes appear for La_{0.3}Sr_{2.7}Ni₂O₅Cl₂ in our first-principles calculation. On the other hand, hole doping is not good for superconductivity.

In Fig. 4, we plot the gap function in the band representation for Sr₃Ni₂O₅Cl₂ ($\Delta n = 0.01$) and La₃Ni₂O₇ ($\Delta n = 0$). For Sr₃Ni₂O₅Cl₂, the gap function of the $d_{3z^2-r^2}$ portion of the band is large with a basically $s\pm$ -wave structure, i.e., $-$ sign in the bonding and $+$ sign in the antibonding band, as in La₃Ni₂O₇. The gap function of the $d_{x^2-y^2}$ portion is smaller compared to La₃Ni₂O₇ due to the smaller hybridization with $d_{3z^2-r^2}$. The sign change between the bonding and antibonding $d_{3z^2-r^2}$

bands corresponds to the dominant contribution of the off-diagonal $d_{3z^2-r^2}$ component in the orbital representation, as shown in Fig. 4(c), which means that the pairing takes place mainly in the interlayer channel.

To understand the origin of the large eigenvalue around stoichiometry for Sr₃Ni₂O₅Cl₂, we plot λ against $n[d_{3z^2-r^2}]$ in the right panel of Fig. 3(c). It can be seen from this figure that the reason for λ being larger than La₃Ni₂O₇ is that $n[d_{3z^2-r^2}]$ for Sr₃Ni₂O₅Cl₂ is closer to unity at stoichiometry. If we compare the two materials at the same $n[d_{3z^2-r^2}]$, λ for Sr₃Ni₂O₅Cl₂ is suppressed compared to that of La₃Ni₂O₇ when $\Delta n < 0$, where the Fermi level intersects the nearly flat band consisting of a mixture of $d_{yz/zx}$ and $d_{3z^2-r^2}$ orbitals. This suppression becomes small when the $t_{2g} - e_g$ interorbital interactions are turned off, suggesting that this interorbital interaction is harmful for superconductivity especially when the t_{2g} orbitals strongly hybridize with the $d_{3z^2-r^2}$ orbital near the Fermi level. This is the origin of the reduction of λ upon hole doping.

Here, we make a brief comment on the robustness of our results against the interaction parameters. We also calculated λ for Sr₃Ni₂O₅Cl₂ at stoichiometry using the interaction parameters evaluated with the constrained random-phase approximation (cRPA) and obtained $\lambda = 0.767$. Although this value is slightly smaller than $\lambda = 0.806$ shown in Fig. 4(c), it is still sufficiently higher than λ for pressurized La₃Ni₂O₇ at stoichiometry. The obtained interaction parameters are shown in Appendix D. We also note that, in our previous study [8], we verified that λ for La₃Ni₂O₇ is similar between two sets of interaction parameters: $(U, U', J = J') = (3, 2.4, 0.3)$ eV and those evaluated with cRPA [11].

Our theoretical analysis illustrates the effect of the mixed-anion strategy of materials design on bilayer nickelate. First of all, the tetragonal structure is stabilized in Sr₃Ni₂O₅Cl₂ as confirmed by our phonon calculation. Second, the Ni- $d_{3z^2-r^2}$ orbital energy is pushed down by the crystal field where a half of apical O²⁻ ions is replaced with a Cl⁻ ion. This results in two opposite effects on superconductivity as follows. The Ni- $d_{3z^2-r^2}$ orbital becomes rather closer to the half-filling in Sr₃Ni₂O₅Cl₂ than La₃Ni₂O₇ whereas the stoichiometric Ni-3d band filling are decreased in Sr₃Ni₂O₅Cl₂ (d^7) compared with La₃Ni₂O₇ ($d^{7.5}$). The increase of the Ni- $d_{3z^2-r^2}$ band filling is beneficial for superconductivity, which was also discussed for La₃Ni₂O₇ in our previous study [8]. On the other hand, the lowered Ni- $d_{3z^2-r^2}$ orbital energy together with the low-symmetry crystal field enhances the hybridization between the t_{2g} and e_g orbitals, which is detrimental for superconductivity. In total, we have seen that Sr₃Ni₂O₅Cl₂ is a promising new candidate of bilayer-nickelate superconductors, which can possess even higher T_c than pressurized La₃Ni₂O₇, at ambient pressure.

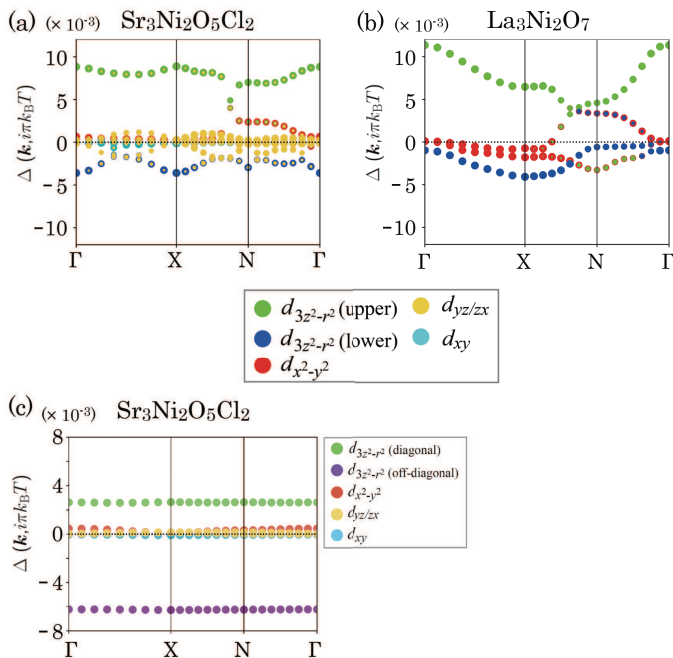


FIG. 4. (a) The superconducting gap function for $\text{Sr}_3\text{Ni}_2\text{O}_5\text{Cl}_2$ ($\Delta n = 0.01$) at $T = 0.01$ eV in the band representation, compared with (b) that for the four-orbital model of $\text{La}_3\text{Ni}_2\text{O}_7$ ($\Delta n = 0$). The strength of the Wannier orbital characters is shown with the radius of the color coded circles, where the weight of the $d_{3z^2-r^2}$ orbital is indicated by either green or blue, depending on whether the band energy is above or below $E = 0.1$ eV. (c) Same as (a) but in the orbital representation, where the orbital-diagonal components for all d orbitals and the orbital-off-diagonal component for the $d_{3z^2-r^2}$ orbital are shown.

D. Formation energy (enthalpy)

To examine the possibility for the synthesis of $\text{Sr}_3\text{Ni}_2\text{O}_5\text{Cl}_2$, we calculated formation energies for some possible chemical reactions as presented in Table II. Here, the formation energy is defined as the total energy of the right-hand side of the chemical equation relative to that for the left-hand side. Huge (negative) formation energies for reactions (a)(b) mean that the left-hand sides of (a)(b) are very unstable and unlikely the final products after the chemical reaction, while they are perhaps good starting points to promote the chemical reaction. On the other hand, we found that $\text{Sr}_2\text{NiO}_2\text{Cl}_2 + \text{SrNiO}_3$ and $\text{SrNiO}_3 + \text{SrNiO}_2 + \text{SrCl}_2$ have similar total energies to that of the target compound $\text{Sr}_3\text{Ni}_2\text{O}_5\text{Cl}_2$. This result suggests that, even by starting from the relatively unstable compounds including SrO_2 , which was used in synthesis of similar oxychlorides, $\text{Sr}_2\text{NiO}_2\text{Cl}_2$ [100], $\text{Sr}_2\text{CoO}_3\text{Cl}$, and $\text{Sr}_3\text{Co}_2\text{O}_5\text{Cl}_2$ [80], a synthesis can be trapped in the middle of the reaction.

However, this problem might be resolved by the high-pressure synthesis, as adopted in Ref. 100 for $\text{Sr}_2\text{NiO}_2\text{Cl}_2$. Figure 5 presents that the formation en-

TABLE II. Formation energies of $\text{Sr}_3\text{Ni}_2\text{O}_5\text{Cl}_2$.

	(meV)
(a) $2\text{SrO}_2 + \text{SrCl}_2 + 2\text{Ni} + \frac{1}{2}\text{O}_2 \rightarrow \text{Sr}_3\text{Ni}_2\text{O}_5\text{Cl}_2$	-5223
(b) $\text{SrO}_2 + \text{SrO} + \text{SrCl}_2 + 2\text{NiO} \rightarrow \text{Sr}_3\text{Ni}_2\text{O}_5\text{Cl}_2$	-2523
(c) $\text{Sr}_2\text{NiO}_2\text{Cl}_2 + \text{SrNiO}_3 \rightarrow \text{Sr}_3\text{Ni}_2\text{O}_5\text{Cl}_2$	-46
(d) $\text{SrNiO}_3 + \text{SrNiO}_2 + \text{SrCl}_2 \rightarrow \text{Sr}_3\text{Ni}_2\text{O}_5\text{Cl}_2$	3

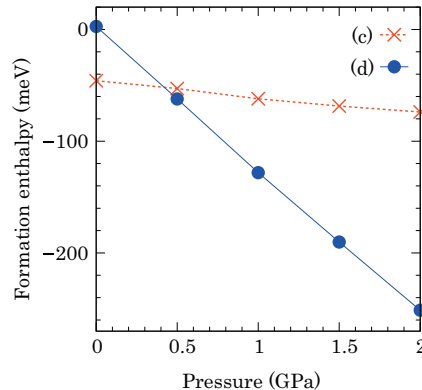


FIG. 5. Formation enthalpy of chemical reactions (c)(d) defined in Table II.

thalpy with respect to the applied pressure for chemical reactions (c)(d) that are defined in Table II. Here, the enthalpy is defined as the sum of the total energy and the pV term, where p and V are the pressure and the volume, respectively. We found that the formation enthalpy goes to negative even for reaction (d).

Therefore, we can expect that the material we proposed in this study, $\text{Sr}_3\text{Ni}_2\text{O}_5\text{Cl}_2$, can be synthesized with a help of the high-pressure synthesis. Our calculation also suggests that, under sufficiently high pressure, $\text{Sr}_2\text{NiO}_2\text{Cl}_2$ can appear as impurity phases because the formation enthalpy for chemical reaction (c) is not effectively lowered by pressure as shown in Fig. 5. This result suggests that $\text{Sr}_2\text{NiO}_2\text{Cl}_2$ is possibly included as an impurity phase in the high-pressure synthesis of $\text{Sr}_3\text{Ni}_2\text{O}_5\text{Cl}_2$ under some conditions.

IV. SUMMARY

We have theoretically investigated the electronic structure of $\text{Sr}_3\text{Ni}_2\text{O}_5\text{Cl}_2$ and its structural stability. Our phonon calculation has shown that this compound with the $I4/mmm$ tetragonal structure is dynamically stable, i.e., does not have imaginary-frequency phonon modes, even at ambient pressure. The Ni- $d_{3z^2-r^2}$ orbital energy is pushed down by the crystal field where a half of apical O^{2-} ions is replaced with a Cl^- ion. By this effect, the Ni- $d_{3z^2-r^2}$ orbital becomes rather closer to the half-filling in $\text{Sr}_3\text{Ni}_2\text{O}_5\text{Cl}_2$ than $\text{La}_3\text{Ni}_2\text{O}_7$ whereas the stoichiometric Ni-3d band filling are decreased in $\text{Sr}_3\text{Ni}_2\text{O}_5\text{Cl}_2$ (d^7) compared with $\text{La}_3\text{Ni}_2\text{O}_7$ ($d^{7.5}$).

By investigating superconductivity with the multi-orbital Hubbard model using the FLEX approximation

combined with the linearized Eliashberg equation, we have found two features originating from the characteristic crystal field. First, interorbital interactions between the t_{2g} and e_g orbitals are detrimental for superconductivity. On the other hand, a nearly half-filled Ni- $d_{3z^2-r^2}$ orbital enhances superconductivity. In total, we have found that $\text{Sr}_3\text{Ni}_2\text{O}_5\text{Cl}_2$ is a promising new candidate of bilayer-nickelate superconductors, which can possess even higher T_c than pressurized $\text{La}_3\text{Ni}_2\text{O}_7$, at ambient pressure. By calculating the formation enthalpy, we have found that the high-pressure synthesis can be a good way to actually produce $\text{Sr}_3\text{Ni}_2\text{O}_5\text{Cl}_2$.

It is noteworthy that the bilayer band structure consisting of Ni- $d_{3z^2-r^2}$ orbitals has a quite small bandwidth with a large bilayer splitting energy in $\text{Sr}_3\text{Ni}_2\text{O}_5\text{Cl}_2$. Namely, the present system perhaps lies in the strong-coupling regime of the bilayer square lattice, where the interlayer superexchange interaction J_\perp stronger than the intralayer hopping amplitudes can enhance the superconductivity [104]. This aspect can already be seen in $\text{La}_3\text{Ni}_2\text{O}_7$, but is more pronounced in the present system. Thus, it is an intriguing future problem to investigate the present system from a strong-coupling picture.

Our study offers an important knowledge for materials design of bilayer-nickelate superconductors and will stimulate experimental investigation of mixed-anion bilayer-nickelate superconductors.

ACKNOWLEDGMENTS

We thank Yoshihiko Takano, Hiroya Sakurai, and Kazuki Yamane for fruitful discussions. This study was supported by JSPS KAKENHI Grant No. JP22K03512, JP22K04907, and JP24K01333. Part of computation was performed using the facilities of the Supercomputer Center, the Institute for Solid State Physics, the University of Tokyo, Japan, and Academic Center for Computing and Media Studies, Kyoto University, Japan.

APPENDIX A: PHONON BAND DISPERSION FOR $\text{La}_3\text{Ni}_2\text{O}_7$

Figure 6 presents the calculated phonon dispersion for $\text{La}_3\text{Ni}_2\text{O}_7$ under 0 and 20 GPa. We confirmed that the crystal structure with the $I4/mmm$ space group is unstable without applying the pressure but is stable by applying a sufficient pressure as reported in several studies [32, 41, 42].

APPENDIX B: PHONON BAND DISPERSION FOR $\text{Sr}_3\text{Ni}_2\text{O}_4\text{Cl}_3$

Figure 7 presents the crystal structure and the calculated phonon dispersion for $\text{Sr}_3\text{Ni}_2\text{O}_4\text{Cl}_3$, where all the apical oxygens were replaced with chlorines. We found

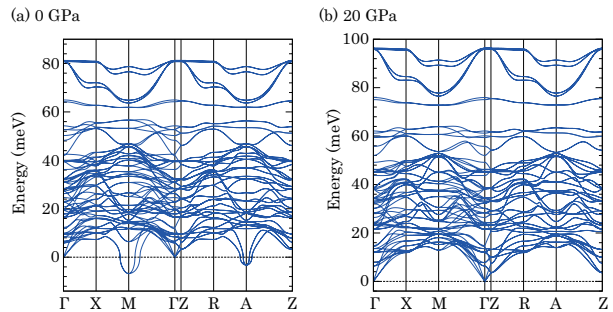


FIG. 6. Phonon band dispersion for $\text{La}_3\text{Ni}_2\text{O}_7$ at (a) 0 GPa and (b) 20 GPa, respectively.

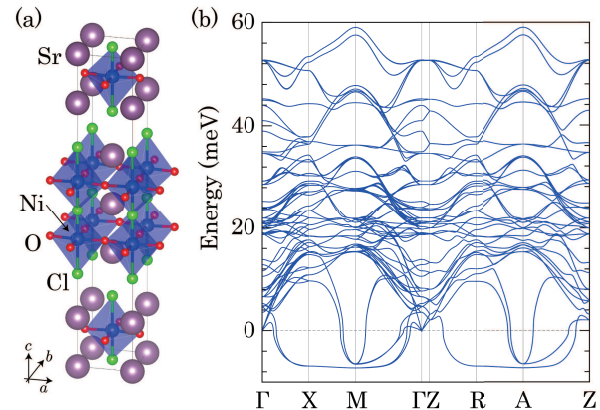


FIG. 7. (a) Crystal structure and (b) phonon band dispersion for $\text{Sr}_3\text{Ni}_2\text{O}_4\text{Cl}_3$.

that the crystal structure with the $I4/mmm$ space group is unstable for this material because imaginary-frequency phonon modes appear in Fig. 7(b).

APPENDIX C: ELECTRONIC AND PHONON BAND STRUCTURES FOR $\text{La}_{0.3}\text{Sr}_{2.7}\text{Ni}_2\text{O}_5\text{Cl}_2$

Figure 8 presents the electronic band structure and the phonon dispersion for $\text{La}_{0.3}\text{Sr}_{2.7}\text{Ni}_2\text{O}_5\text{Cl}_2$, where the La doping was handled with the virtual crystal approximation. We found that the rigid-band approximation adopted in this study was justified in Fig. 8(a) because the electronic band dispersion for $\text{La}_{0.3}\text{Sr}_{2.7}\text{Ni}_2\text{O}_5\text{Cl}_2$ agrees well with that for $\text{Sr}_3\text{Ni}_2\text{O}_5\text{Cl}_2$ with a shifted Fermi energy. In addition, the absence of the imaginary-frequency phonon modes in Fig. 8(b) suggests that the stability of the $I4/mmm$ structure is kept against the La doping.

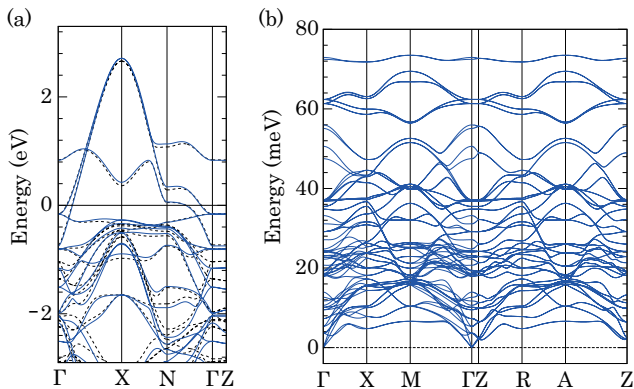


FIG. 8. (a) Electronic band structure for $\text{La}_{0.3}\text{Sr}_{2.7}\text{Ni}_2\text{O}_5\text{Cl}_2$ (blue solid lines) shown together with that for $\text{Sr}_3\text{Ni}_2\text{O}_5\text{Cl}_2$ with a shifted Fermi energy (black broken lines). (b) Phonon band dispersion for $\text{La}_{0.3}\text{Sr}_{2.7}\text{Ni}_2\text{O}_5\text{Cl}_2$.

APPENDIX D: CRPA INTERACTION PARAMETERS FOR $\text{Sr}_3\text{Ni}_2\text{O}_5\text{Cl}_2$

We evaluated the onsite interaction parameters for the ten-orbital model of $\text{Sr}_3\text{Ni}_2\text{O}_5\text{Cl}_2$ using the cRPA [105] with the projector method [106]. For this purpose, we used the plane-wave cutoff energy of 450 eV, 200 bands

including occupied and unoccupied states, and an $8 \times 8 \times 8$ \mathbf{k} -mesh. Obtained interaction parameters are shown in Table III.

TABLE III. Interaction parameters of onsite Coulomb repulsion U, U' and Hund's coupling (pair-hopping) $J (J')$ evaluated with cRPA. The orbital indices $l, m = 1, 2, 3, 4, 5$ indicate the $d_{x^2-y^2}, d_{3z^2-r^2}, d_{xy}, d_{yz}, d_{zx}$ orbitals, respectively. For simplicity, we abbreviate four-orbital-index-representation of partially screened interaction integrals V , namely, $V_{llmm} \rightarrow U'_{lm}$ and $V_{lmlm} (= V_{lmm}) \rightarrow J_{lm}$. Note that $U'_{lm} = U'_{ml}$, $J_{lm} = J_{ml}$, and $J_{lm} = J'_{lm}$. All in eV.

l, m	U, U'	J, J'
1, 1	3.936	—
1, 2	2.866	0.563
1, 3	3.151	0.249
1, 4	2.990	0.473
1, 5	2.990	0.473
2, 2	4.080	—
2, 3	2.683	0.460
2, 4	3.365	0.347
2, 5	3.365	0.347
3, 3	3.393	—
3, 4	2.802	0.420
3, 5	2.802	0.420
4, 4	4.088	—
4, 5	3.040	0.472
5, 5	4.088	—

- [1] H. Sun, M. Huo, X. Hu, J. Li, Z. Liu, Y. Han, L. Tang, Z. Mao, P. Yang, B. Wang, J. Cheng, D.-X. Yao, G.-M. Zhang, and M. Wang, Signatures of superconductivity near 80 K in a nickelate under high pressure, *Nature* **621**, 493 (2023).
- [2] Z. Ouyang, M. Gao, and Z.-Y. Lu, Absence of electron-phonon coupling superconductivity in the bilayer phase of $\text{La}_3\text{Ni}_2\text{O}_7$ under pressure, *npj Quantum Mater.* **9**, 80 (2024).
- [3] Y. D. Li, Y. T. Cao, L. Y. Liu, P. Peng, H. Lin, C. Y. Pei, M. X. Zhang, H. Wu, X. Du, W. X. Zhao, K. Y. Zhai, J. K. Zhao, M.-L. Lin, P. H. Tan, Y. P. Qi, G. Li, H. J. Guo, L. Yang, and L. X. Yang, Ultrafast Dynamics of Bilayer and Trilayer Nickelate Superconductors, arXiv:2403.05012 (2024).
- [4] X.-W. Yi, Y. Meng, J.-W. Li, Z.-W. Liao, W. Li, J.-Y. You, B. Gu, and G. Su, Nature of charge density waves and metal-insulator transition in pressurized $\text{La}_3\text{Ni}_2\text{O}_7$, *Phys. Rev. B* **110**, L140508 (2024).
- [5] Y. Zhang, L.-F. Lin, A. Moreo, and E. Dagotto, Electronic structure, dimer physics, orbital-selective behavior, and magnetic tendencies in the bilayer nickelate superconductor $\text{La}_3\text{Ni}_2\text{O}_7$ under pressure, *Phys. Rev. B* **108**, L180510 (2023).
- [6] Q.-G. Yang, D. Wang, and Q.-H. Wang, Possible s_{\pm} -wave superconductivity in $\text{La}_3\text{Ni}_2\text{O}_7$, *Phys. Rev. B* **108**, L140505 (2023).
- [7] F. Lechermann, J. Gondolf, S. Bötzel, and I. M. Eremin, Electronic correlations and superconducting instability in $\text{La}_3\text{Ni}_2\text{O}_7$ under high pressure, *Phys. Rev. B* **108**, L201121 (2023).
- [8] H. Sakakibara, N. Kitamine, M. Ochi, and K. Kuroki, Possible high T_c superconductivity in $\text{La}_3\text{Ni}_2\text{O}_7$ under high pressure through manifestation of a nearly half-filled bilayer Hubbard model, *Phys. Rev. Lett.* **132**, 106002 (2024).
- [9] Y. Gu, C. Le, Z. Yang, X. Wu, and J. Hu, Effective model and pairing tendency in bilayer Ni-based superconductor $\text{La}_3\text{Ni}_2\text{O}_7$, arXiv:2306.07275 (2023).
- [10] Y. Shen, M. Qin, and G.-M. Zhang, Effective bi-layer model hamiltonian and density-matrix renormalization group study for the high- T_c superconductivity in $\text{La}_3\text{Ni}_2\text{O}_7$ under high pressure, *Chin. Phys. Lett.* **40**, 127401 (2023).
- [11] V. Christiansson, F. Petocchi, and P. Werner, Correlated electronic structure of $\text{La}_3\text{Ni}_2\text{O}_7$ under pressure, *Phys. Rev. Lett.* **131**, 206501 (2023).
- [12] Z. Liu, M. Huo, J. Li, Q. Li, Y. Liu, Y. Dai, X. Zhou, J. Hao, Y. Lu, M. Wang, and H.-H. Wen, Electronic correlations and partial gap in the bilayer nickelate $\text{La}_3\text{Ni}_2\text{O}_7$, *Nat. Commun.* **15**, 7570 (2024).
- [13] W. Wú, Z. Luo, D.-X. Yao, and M. Wang, Superexchange and charge transfer in the nickelate superconductor $\text{La}_3\text{Ni}_2\text{O}_7$ under pressure, *Sci. China Phys. Mech. Astron.* **67**, 117402 (2024).
- [14] Y. Cao and Y.-f. Yang, Flat bands promoted by hund's rule coupling in the candidate double-layer high-temperature superconductor $\text{La}_3\text{Ni}_2\text{O}_7$ under high pres-

- sure, Phys. Rev. B **109**, L081105 (2024).
- [15] J. Hou, P.-T. Yang, Z.-Y. Liu, J.-Y. Li, P.-F. Shan, L. Ma, G. Wang, N.-N. Wang, H.-Z. Guo, J.-P. Sun, Y. Uwatoko, M. Wang, G.-M. Zhang, B.-S. Wang, and J.-G. Cheng, Emergence of high-temperature superconducting phase in pressurized $\text{La}_3\text{Ni}_2\text{O}_7$ crystals, Chin. Phys. Lett. **40**, 117302 (2023).
- [16] Y.-B. Liu, J.-W. Mei, F. Ye, W.-Q. Chen, and F. Yang, s^\pm -wave pairing and the destructive role of apical-oxygen deficiencies in $\text{La}_3\text{Ni}_2\text{O}_7$ under pressure, Phys. Rev. Lett. **131**, 236002 (2023).
- [17] Y. Zhang, D. Su, Y. Huang, Z. Shan, H. Sun, M. Huo, K. Ye, J. Zhang, Z. Yang, Y. Xu, Y. Su, R. Li, M. Smidman, M. Wang, L. Jiao, and H. Yuan, High-temperature superconductivity with zero resistance and strange-metal behaviour in $\text{La}_3\text{Ni}_2\text{O}_{7-\delta}$, Nat. Phys. **20**, 1269 (2024).
- [18] C. Lu, Z. Pan, F. Yang, and C. Wu, Interlayer-coupling-driven high-temperature superconductivity in $\text{La}_3\text{Ni}_2\text{O}_7$ under pressure, Phys. Rev. Lett. **132**, 146002 (2024).
- [19] Y. Zhang, L.-F. Lin, A. Moreo, T. A. Maier, and E. Dagotto, Structural phase transition, s_\pm -wave pairing, and magnetic stripe order in bilayered superconductor $\text{La}_3\text{Ni}_2\text{O}_7$ under pressure, Nat. Commun. **15**, 2470 (2024).
- [20] H. Oh and Y.-H. Zhang, Type-II $t-J$ model and shared superexchange coupling from Hund's rule in superconducting $\text{La}_3\text{Ni}_2\text{O}_7$, Phys. Rev. B **108**, 174511 (2023).
- [21] Z. Liao, L. Chen, G. Duan, Y. Wang, C. Liu, R. Yu, and Q. Si, Electron correlations and superconductivity in $\text{La}_3\text{Ni}_2\text{O}_7$ under pressure tuning, Phys. Rev. B **108**, 214522 (2023).
- [22] X.-Z. Qu, D.-W. Qu, J. Chen, C. Wu, F. Yang, W. Li, and G. Su, Bilayer $t-J-J_\perp$ model and magnetically mediated pairing in the pressurized nickelate $\text{La}_3\text{Ni}_2\text{O}_7$, Phys. Rev. Lett. **132**, 036502 (2024).
- [23] Y.-f. Yang, G.-M. Zhang, and F.-C. Zhang, Interlayer valence bonds and two-component theory for high- T_c superconductivity of $\text{La}_3\text{Ni}_2\text{O}_7$ under pressure, Phys. Rev. B **108**, L201108 (2023).
- [24] K. Jiang, Z. Wang, and F.-C. Zhang, High-temperature superconductivity in $\text{La}_3\text{Ni}_2\text{O}_7$, Chin. Phys. Lett. **41**, 017402 (2024).
- [25] Y. Zhang, L.-F. Lin, A. Moreo, T. A. Maier, and E. Dagotto, Trends in electronic structures and s_\pm -wave pairing for the rare-earth series in bilayer nickelate superconductor $R_3\text{Ni}_2\text{O}_7$, Phys. Rev. B **108**, 165141 (2023).
- [26] Y.-H. Tian, Y. Chen, J.-M. Wang, R.-Q. He, and Z.-Y. Lu, Correlation effects and concomitant two-orbital s_\pm -wave superconductivity in $\text{La}_3\text{Ni}_2\text{O}_7$ under high pressure, Phys. Rev. B **109**, 165154 (2024).
- [27] R. Jiang, J. Hou, Z. Fan, Z.-J. Lang, and W. Ku, Pressure driven fractionalization of ionic spins results in cupratelike high- T_c superconductivity in $\text{La}_3\text{Ni}_2\text{O}_7$, Phys. Rev. Lett. **132**, 126503 (2024).
- [28] Z. Luo, B. Lv, M. Wang, W. Wú, and D.-X. Yao, High- T_c superconductivity in $\text{La}_3\text{Ni}_2\text{O}_7$ based on the bilayer two-orbital $t-J$ model, npj Quantum Mater. **9**, 61 (2024).
- [29] J. Yang, H. Sun, X. Hu, Y. Xie, T. Miao, H. Luo, H. Chen, B. Liang, W. Zhu, G. Qu, C.-Q. Chen, M. Huo, Y. Huang, S. Zhang, F. Zhang, F. Yang, Z. Wang, Q. Peng, H. Mao, G. Liu, Z. Xu, T. Qian, D.-X. Yao, M. Wang, L. Zhao, and X. J. Zhou, Orbital-dependent electron correlation in double-layer nickelate $\text{La}_3\text{Ni}_2\text{O}_7$, Nat. Commun. **15**, 4373 (2024).
- [30] M. Zhang, C. Pei, Q. Wang, Y. Zhao, C. Li, W. Cao, S. Zhu, J. Wu, and Y. Qi, Effects of pressure and doping on Ruddlesden-Popper phases $\text{La}_{n+1}\text{Ni}_n\text{O}_{3n+1}$, J. Mater. Sci. Technol. **185**, 147 (2024).
- [31] H. Sakakibara, M. Ochi, H. Nagata, Y. Ueki, H. Sakurai, R. Matsumoto, K. Terashima, K. Hirose, H. Ohta, M. Kato, Y. Takano, and K. Kuroki, Theoretical analysis on the possibility of superconductivity in the trilayer Ruddlesden-Popper nickelate $\text{La}_4\text{Ni}_3\text{O}_{10}$ under pressure and its experimental examination: Comparison with $\text{La}_3\text{Ni}_2\text{O}_7$, Phys. Rev. B **109**, 144511 (2024).
- [32] B. Geisler, J. J. Hamlin, G. R. Stewart, R. G. Hennig, and P. J. Hirschfeld, Structural transitions, octahedral rotations, and electronic properties of $\text{A}_3\text{Ni}_2\text{O}_7$ rare-earth nickelates under high pressure, npj Quantum Mater. **9**, 38 (2024).
- [33] L. C. Rhodes and P. Wahl, Structural routes to stabilize superconducting $\text{La}_3\text{Ni}_2\text{O}_7$ at ambient pressure, Phys. Rev. Mater. **8**, 044801 (2024).
- [34] G. Wang, N. N. Wang, X. L. Shen, J. Hou, L. Ma, L. F. Shi, Z. A. Ren, Y. D. Gu, H. M. Ma, P. T. Yang, Z. Y. Liu, H. Z. Guo, J. P. Sun, G. M. Zhang, S. Calder, J.-Q. Yan, B. S. Wang, Y. Uwatoko, and J.-G. Cheng, Pressure-induced superconductivity in polycrystalline $\text{La}_3\text{Ni}_2\text{O}_{7-\delta}$, Phys. Rev. X **14**, 011040 (2024).
- [35] T. Kaneko, H. Sakakibara, M. Ochi, and K. Kuroki, Pair correlations in the two-orbital Hubbard ladder: Implications for superconductivity in the bilayer nickelate $\text{La}_3\text{Ni}_2\text{O}_7$, Phys. Rev. B **109**, 045154 (2024).
- [36] C. Lu, Z. Pan, F. Yang, and C. Wu, Interplay of two E_g orbitals in superconducting $\text{La}_3\text{Ni}_2\text{O}_7$ under pressure, Phys. Rev. B **110**, 094509 (2024).
- [37] S. Ryee, N. Witt, and T. O. Wehling, Quenched pair breaking by interlayer correlations as a key to superconductivity in $\text{La}_3\text{Ni}_2\text{O}_7$, Phys. Rev. Lett. **133**, 096002 (2024).
- [38] Q. Li, Y.-J. Zhang, Z.-N. Xiang, Y. Zhang, X. Zhu, and H.-H. Wen, Signature of superconductivity in pressurized $\text{La}_4\text{Ni}_3\text{O}_{10}$, Chin. Phys. Lett. **41**, 017401 (2024).
- [39] Y. Zhu, D. Peng, E. Zhang, B. Pan, X. Chen, L. Chen, H. Ren, F. Liu, Y. Hao, N. Li, Z. Xing, F. Lan, J. Han, J. Wang, D. Jia, H. Wo, Y. Gu, Y. Gu, L. Ji, W. Wang, H. Gou, Y. Shen, T. Ying, X. Chen, W. Yang, H. Cao, C. Zheng, Q. Zeng, J.-G. Guo, and J. Zhao, Superconductivity in pressurized trilayer $\text{La}_4\text{Ni}_3\text{O}_{10-\delta}$ single crystals, Nature **631**, 531 (2024).
- [40] M. Zhang, C. Pei, X. Du, W. Hu, Y. Cao, Q. Wang, J. Wu, Y. Li, H. Liu, C. Wen, Y. Zhao, C. Li, W. Cao, S. Zhu, Q. Zhang, N. Yu, P. Cheng, L. Zhang, Z. Li, J. Zhao, Y. Chen, H. Guo, C. Wu, F. Yang, S. Yan, L. Yang, and Y. Qi, Superconductivity in trilayer nickelate $\text{La}_4\text{Ni}_3\text{O}_{10}$ under pressure, arXiv:2311.07423 (2023).
- [41] G. Wang, N. Wang, Y. Wang, L. Shi, X. Shen, J. Hou, H. Ma, P. Yang, Z. Liu, H. Zhang, X. Dong, J. Sun, B. Wang, K. Jiang, J. Hu, Y. Uwatoko, and J. Cheng, Observation of high-temperature superconductivity in the high-pressure tetragonal phase of $\text{La}_2\text{PrNi}_2\text{O}_{7-\delta}$, arXiv:2311.08212 (2023).
- [42] L. Wang, Y. Li, S.-Y. Xie, F. Liu, H. Sun, C. Huang, Y. Gao, T. Nakagawa, B. Fu, B. Dong, Z. Cao, R. Yu, S. I. Kawaguchi, H. Kadobayashi,

- M. Wang, C. Jin, H.-k. Mao, and H. Liu, Structure responsible for the superconducting state in $\text{La}_3\text{Ni}_2\text{O}_7$ at high-pressure and low-temperature conditions, *J. Am. Chem. Soc.* **146**, 7506 (2024).
- [43] Z. Ouyang, J.-M. Wang, J.-X. Wang, R.-Q. He, L. Huang, and Z.-Y. Lu, Hund electronic correlation in $\text{La}_3\text{Ni}_2\text{O}_7$ under high pressure, *Phys. Rev. B* **109**, 115114 (2024).
- [44] N. Yuan, A. Elghandour, J. Arneth, K. Dey, and R. Klingeler, High-pressure crystal growth and investigation of the metal-to-metal transition of Ruddlesden-Popper trilayer nickelates $\text{La}_4\text{Ni}_3\text{O}_{10}$, *J. Cryst. Growth* **627**, 127511 (2024).
- [45] Y. Zhou, J. Guo, S. Cai, H. Sun, P. Wang, J. Zhao, J. Han, X. Chen, Y. Chen, Q. Wu, Y. Ding, T. Xiang, H.-K. Mao, and L. Sun, Investigations of key issues on the reproducibility of high- T_c superconductivity emerging from compressed $\text{La}_3\text{Ni}_2\text{O}_7$, arXiv:2311.12361 (2023).
- [46] X.-Z. Qu, D.-W. Qu, W. Li, and G. Su, Roles of Hund's Rule and Hybridization in the Two-orbital Model for High- T_c Superconductivity in the Bilayer Nickelate, arXiv:2311.12769 (2023).
- [47] K. Chen, X. Liu, J. Jiao, M. Zou, C. Jiang, X. Li, Y. Luo, Q. Wu, N. Zhang, Y. Guo, and L. Shu, Evidence of spin density waves in $\text{La}_3\text{Ni}_2\text{O}_{7-\delta}$, *Phys. Rev. Lett.* **132**, 256503 (2024).
- [48] J. Li, C.-Q. Chen, C. Huang, Y. Han, M. Huo, X. Huang, P. Ma, Z. Qiu, J. Chen, X. Hu, L. Chen, T. Xie, B. Shen, H. Sun, D.-X. Yao, and M. Wang, Structural transition, electric transport, and electronic structures in the compressed trilayer nickelate $\text{La}_4\text{Ni}_3\text{O}_{10}$, *Sci. China Phys. Mech. Astron.* **67**, 117403 (2024).
- [49] X. Sui, X. Han, H. Jin, X. Chen, L. Qiao, X. Shao, and B. Huang, Electronic properties of the bilayer nickelates $R_3\text{Ni}_2\text{O}_7$ with oxygen vacancies ($R = \text{La}$ or Ce), *Phys. Rev. B* **109**, 205156 (2024).
- [50] M. Kakoi, T. Kaneko, H. Sakakibara, M. Ochi, and K. Kuroki, Pair correlations of the hybridized orbitals in a ladder model for the bilayer nickelate $\text{La}_3\text{Ni}_2\text{O}_7$, *Phys. Rev. B* **109**, L201124 (2024).
- [51] X. Chen, J. Zhang, A. S. Thind, S. Sharma, H. LaBollita, G. Peterson, H. Zheng, D. P. Phelan, A. S. Botana, R. F. Klie, and J. F. Mitchell, Polymorphism in the Ruddlesden-Popper nickelate $\text{La}_3\text{Ni}_2\text{O}_7$: Discovery of a hidden phase with distinctive layer stacking, *J. Am. Chem. Soc.* **146**, 3640 (2024).
- [52] P. Puphal, P. Reiss, N. Enderlein, Y.-M. Wu, G. Khalullin, V. Sundaramurthy, T. Priessnitz, M. Knauff, A. Suthar, L. Richter, M. Isobe, P. A. van Aken, H. Takagi, B. Keimer, Y. E. Suyolcu, B. Wehinger, P. Hansmann, and M. Hepting, Unconventional crystal structure of the high-pressure superconductor $\text{La}_3\text{Ni}_2\text{O}_7$, *Phys. Rev. Lett.* **133**, 146002 (2024).
- [53] F. Li, N. Guo, Q. Zheng, Y. Shen, S. Wang, Q. Cui, C. Liu, S. Wang, X. Tao, G.-M. Zhang, and J. Zhang, Design and synthesis of three-dimensional hybrid Ruddlesden-Popper nickelate single crystals, *Phys. Rev. Mater.* **8**, 053401 (2024).
- [54] H. Wang, L. Chen, A. Rutherford, H. Zhou, and W. Xie, Long-range structural order in a hidden phase of Ruddlesden-Popper bilayer nickelate $\text{La}_3\text{Ni}_2\text{O}_7$, *Inorg. Chem.* **63**, 5020 (2024).
- [55] M. Kakoi, T. Oi, Y. Ohshita, M. Yashima, K. Kuroki, T. Kato, H. Takahashi, S. Ishiwata, Y. Adachi, N. Hatada, T. Uda, and H. Mukuda, Multiband metallic ground state in multilayered nickelates $\text{La}_3\text{Ni}_2\text{O}_7$ and $\text{La}_4\text{Ni}_3\text{O}_{10}$ probed by ^{139}La -NMR at ambient pressure, *J. Phys. Soc. Jpn.* **93**, 053702 (2024).
- [56] Z. Dong, M. Huo, J. Li, J. Li, P. Li, H. Sun, L. Gu, Y. Lu, M. Wang, Y. Wang, and Z. Chen, Visualization of oxygen vacancies and self-doped ligand holes in $\text{La}_3\text{Ni}_2\text{O}_{7-\delta}$, *Nature* **630**, 847 (2024).
- [57] Strong interlayer magnetic exchange coupling in $\text{La}_3\text{Ni}_2\text{O}_{7-\delta}$ revealed (2024).
- [58] X. Chen, J. Choi, Z. Jiang, J. Mei, K. Jiang, J. Li, S. Agrestini, M. Garcia-Fernandez, H. Sun, X. Huang, D. Shen, M. Wang, J. Hu, Y. Lu, K.-J. Zhou, and D. Feng, Electronic and magnetic excitations in $\text{La}_3\text{Ni}_2\text{O}_7$, *Nat. Commun.* **15**, 9597 (2024).
- [59] Y. Wang, K. Jiang, Z. Wang, F.-C. Zhang, and J. Hu, Electronic and magnetic structures of bilayer $\text{La}_3\text{Ni}_2\text{O}_7$ at ambient pressure, *Phys. Rev. B* **110**, 205122 (2024).
- [60] P.-F. Tian, H.-T. Ma, X. Ming, X.-J. Zheng, and H. Li, Effective model and electron correlations in trilayer nickelate superconductor $\text{La}_4\text{Ni}_3\text{O}_{10}$, *J. Phys.: Cond. Matter* **36**, 355602 (2024).
- [61] J.-X. Wang, Z. Ouyang, R.-Q. He, and Z.-Y. Lu, Non-Fermi liquid and Hund correlation in $\text{La}_4\text{Ni}_3\text{O}_{10}$ under high pressure, *Phys. Rev. B* **109**, 165140 (2024).
- [62] Z. Dan, Y. Zhou, M. Huo, Y. Wang, L. Nie, M. Wang, T. Wu, and X. Chen, Spin-density-wave transition in double-layer nickelate $\text{La}_3\text{Ni}_2\text{O}_7$, arXiv:2402.03952 (2024).
- [63] H. LaBollita, J. Kapeghian, M. R. Norman, and A. S. Botana, Electronic structure and magnetic tendencies of trilayer $\text{La}_4\text{Ni}_3\text{O}_{10}$ under pressure: Structural transition, molecular orbitals, and layer differentiation, *Phys. Rev. B* **109**, 195151 (2024).
- [64] Y. Zhang, L.-F. Lin, A. Moreo, T. A. Maier, and E. Dagotto, Prediction of s^{\pm} -wave superconductivity enhanced by electronic doping in trilayer nickelates $\text{La}_4\text{Ni}_3\text{O}_{10}$ under pressure, *Phys. Rev. Lett.* **133**, 136001 (2024).
- [65] Q.-G. Yang, K.-Y. Jiang, D. Wang, H.-Y. Lu, and Q.-H. Wang, Effective model and s_{\pm} -wave superconductivity in trilayer nickelate $\text{La}_4\text{Ni}_3\text{O}_{10}$, *Phys. Rev. B* **109**, L220506 (2024).
- [66] C. Lu, Z. Pan, F. Yang, and C. Wu, Superconductivity in $\text{La}_4\text{Ni}_3\text{O}_{10}$ Under Pressure, arXiv: 2402.06450 (2024).
- [67] S. N. Abadi, K.-J. Xu, E. G. Lomeli, P. Puphal, M. Isobe, Y. Zhong, A. V. Fedorov, S.-K. Mo, M. Hashimoto, D.-H. Lu, B. Moritz, B. Keimer, T. P. Devereaux, M. Hepting, and Z.-X. Shen, Electronic structure of the alternating monolayer-trilayer phase of $\text{La}_3\text{Ni}_2\text{O}_7$, arXiv:2402.07143 (2024).
- [68] R. Khasanov, T. J. Hicken, D. J. Gawryluk, L. P. Sorel, S. Bötzel, F. Lechermann, I. M. Eremin, H. Luetkens, and Z. Guguchia, Pressure-Induced Split of the Density Wave Transitions in $\text{La}_3\text{Ni}_2\text{O}_{7-\delta}$, arXiv:2402.10485 (2024).
- [69] S. Wu, Z. Yang, X. Ma, J. Dai, M. Shi, H.-Q. Yuan, H.-Q. Lin, and C. Cao, $\text{Ac}_3\text{Ni}_2\text{O}_7$ and $\text{La}_2\text{AeNi}_2\text{O}_6\text{F}$ ($\text{Ae} = \text{Sr}, \text{Ba}$): Benchmark Materials for Bilayer Nickelate Superconductivity, arXiv:2403.11713 (2024).

- [70] J. Li, P. Ma, H. Zhang, X. Huang, C. Huang, M. Huo, D. Hu, Z. Dong, C. He, J. Liao, X. Chen, T. Xie, H. Sun, and M. Wang, Pressure-driven right-triangle shape superconductivity in bilayer nickelate $\text{La}_3\text{Ni}_2\text{O}_7$, arXiv:2404.11369 (2024).
- [71] Y. Meng, Y. Yang, H. Sun, S. Zhang, J. Luo, M. Wang, F. Hong, X. Wang, and X. Yu, Density-wave-like gap evolution in $\text{La}_3\text{Ni}_2\text{O}_7$ under high pressure revealed by ultrafast optical spectroscopy, arXiv:2404.19678 (2024).
- [72] H. Wang, H. Zhou, and W. Xie, Temperature-dependent Structural Evolution of Ruddlesden-Popper Bilayer Nickelate $\text{La}_3\text{Ni}_2\text{O}_7$, arXiv:2405.08802 (2024).
- [73] S. Xu, C.-Q. Chen, M. Huo, D. Hu, H. Wang, Q. Wu, R. Li, D. Wu, M. Wang, D.-X. Yao, T. Dong, and N. Wang, Origin of the density wave instability in trilayer nickelate $\text{La}_4\text{Ni}_3\text{O}_{10}$ revealed by optical and ultrafast spectroscopy, arXiv:2405.19161 (2024).
- [74] X. Du, Y. D. Li, Y. T. Cao, C. Y. Pei, M. X. Zhang, W. X. Zhao, K. Y. Zhai, R. Z. Xu, Z. K. Liu, Z. W. Li, J. K. Zhao, G. Li, Y. L. Chen, Y. P. Qi, H. J. Guo, and L. X. Yang, Correlated Electronic Structure and Density-Wave Gap in Trilayer Nickelate $\text{La}_4\text{Ni}_3\text{O}_{10}$, arXiv:2405.19853 (2024).
- [75] H. Nagata, H. Sakurai, Y. Ueki, K. Yamane, R. Matsumoto, K. Terashima, K. Hirose, H. Ohta, M. Kato, and Y. Takano, Pressure-induced superconductivity in $\text{La}_4\text{Ni}_3\text{O}_{10+\delta}$ ($\delta = 0.04$ and -0.01), *J. Phys. Soc. Jpn.* **93**, 095003 (2024).
- [76] N. Wang, G. Wang, X. Shen, J. Hou, J. Luo, X. Ma, H. Yang, L. Shi, J. Dou, J. Feng, J. Yang, Y. Shi, Z. Ren, H. Ma, P. Yang, Z. Liu, Y. Liu, H. Zhang, X. Dong, Y. Wang, K. Jiang, J. Hu, S. Nagasaki, K. Kitagawa, S. Calder, J. Yan, J. Sun, B. Wang, R. Zhou, Y. Uwatoko, and J. Cheng, Bulk high-temperature superconductivity in pressurized tetragonal $\text{La}_2\text{PrNi}_2\text{O}_7$, *Nature* **634**, 579 (2024).
- [77] Y. Ueki, H. Sakurai, H. Nagata, K. Yamane, R. Matsumoto, K. Terashima, K. Hirose, H. Ohta, M. Kato, and Y. Takano, Phase diagram of pressure-induced high temperature superconductor $\text{La}_3\text{Ni}_2\text{O}_{7+\delta}$, arXiv:2408.04970 (2024).
- [78] M. Nakata, D. Ogura, H. Usui, and K. Kuroki, Finite-energy spin fluctuations as a pairing glue in systems with coexisting electron and hole bands, *Phys. Rev. B* **95**, 214509 (2017).
- [79] W. Leib and H. Müller-Buschbaum, Ein neues oxohalogenoferrat: $\text{Sr}_3\text{Fe}_2\text{O}_5\text{Cl}_2$, *Z. Anorg. Allg. Chem.* **518**, 115 (1984).
- [80] N. McGlothlin, D. Ho, and R. Cava, $\text{Sr}_3\text{Co}_2\text{O}_5\text{Cl}_2$ and $\text{Sr}_2\text{CoO}_3\text{Cl}$: two layered cobalt oxychlorides, *Mater. Res. Bull.* **35**, 1035 (2000).
- [81] Z. Hiroi, N. Kobayashi, and M. Takano, Probable hole-doped superconductivity without apical oxygens in $(\text{Ca}, \text{Na})_2\text{CuO}_2\text{Cl}_2$, *Nature* **371**, 139 (1994).
- [82] K. Momma and F. Izumi, VESTA3 for three-dimensional visualization of crystal, volumetric and morphology data, *J. Appl. Crystallogr.* **44**, 1272 (2011).
- [83] J. P. Perdew, A. Ruzsinszky, G. I. Csonka, O. A. Vydrov, G. E. Scuseria, L. A. Constantin, X. Zhou, and K. Burke, Restoring the density-gradient expansion for exchange in solids and surfaces, *Phys. Rev. Lett.* **100**, 136406 (2008).
- [84] G. Kresse and D. Joubert, From ultrasoft pseudopotentials to the projector augmented-wave method, *Phys. Rev. B* **59**, 1758 (1999).
- [85] G. Kresse and J. Hafner, Ab initio molecular dynamics for liquid metals, *Phys. Rev. B* **47**, 558 (1993).
- [86] G. Kresse and J. Hafner, Ab initio molecular-dynamics simulation of the liquid-metal-amorphous-semiconductor transition in germanium, *Phys. Rev. B* **49**, 14251 (1994).
- [87] G. Kresse and J. Furthmüller, Efficiency of ab-initio total energy calculations for metals and semiconductors using a plane-wave basis set, *Comput. Mater. Sci.* **6**, 15 (1996).
- [88] G. Kresse and J. Furthmüller, Efficient iterative schemes for ab initio total-energy calculations using a plane-wave basis set, *Phys. Rev. B* **54**, 11169 (1996).
- [89] A. Togo, L. Chaput, T. Tadano, and I. Tanaka, Implementation strategies in phonopy and phono3py, *J. Phys. Condens. Matter* **35**, 353001 (2023).
- [90] A. Togo, First-principles phonon calculations with phonopy and phono3py, *J. Phys. Soc. Jpn.* **92**, 012001 (2023).
- [91] N. Marzari and D. Vanderbilt, Maximally localized generalized Wannier functions for composite energy bands, *Phys. Rev. B* **56**, 12847 (1997).
- [92] I. Souza, N. Marzari, and D. Vanderbilt, Maximally localized Wannier functions for entangled energy bands, *Phys. Rev. B* **65**, 035109 (2001).
- [93] G. Pizzi, V. Vitale, R. Arita, S. Blügel, F. Freimuth, G. Géranton, M. Gibertini, D. Gresch, C. Johnson, T. Koretsune, J. Ibañez Azpiroz, H. Lee, J.-M. Lihm, D. Marchand, A. Marazzo, Y. Mokrousov, J. I. Mustafa, Y. Nohara, Y. Nomura, L. Paulatto, S. Poncé, T. Ponweiser, J. Qiao, F. Thöle, S. S. Tsirkin, M. Wierzbowska, N. Marzari, D. Vanderbilt, I. Souza, A. A. Mostofi, and J. R. Yates, Wannier90 as a community code: new features and applications, *J. Phys.: Cond. Matter* **32**, 165902 (2020).
- [94] N. E. Bickers, D. J. Scalapino, and S. R. White, Conserving approximations for strongly correlated electron systems: Bethe-Salpeter equation and dynamics for the two-dimensional Hubbard model, *Phys. Rev. Lett.* **62**, 961 (1989).
- [95] N. E. Bickers and S. R. White, Conserving approximations for strongly fluctuating electron systems. II. Numerical results and parquet extension, *Phys. Rev. B* **43**, 8044 (1991).
- [96] A. I. Lichtenstein and M. I. Katsnelson, Ab initio calculations of quasiparticle band structure in correlated systems: LDA++ approach, *Phys. Rev. B* **57**, 6884 (1998).
- [97] K. Yada and H. Kontani, Origin of weak pseudogap behaviors in $\text{Na}_{0.35}\text{CoO}_2$: Absence of small hole pockets, *J. Phys. Soc. Jpn.* **74**, 2161 (2005).
- [98] M. Mochizuki, Y. Yanase, and M. Ogata, Ferromagnetic fluctuation and possible triplet superconductivity in $\text{Na}_x\text{CoO}_2 \cdot y\text{H}_2\text{O}$: Fluctuation-exchange study of the multiorbital Hubbard model, *Phys. Rev. Lett.* **94**, 147005 (2005).
- [99] H. Ikeda, R. Arita, and J. Kuneš, Phase diagram and gap anisotropy in iron-pnictide superconductors, *Phys. Rev. B* **81**, 054502 (2010).
- [100] Y. Tsujimoto, C. I. Sathish, Y. Matsushita, K. Yamamura, and T. Uchikoshi, New members of layered

- oxychloride perovskites with square planar coordination: $\text{Sr}_2\text{MO}_2\text{Cl}_2$ ($M = \text{Mn}, \text{Ni}$) and $\text{Ba}_2\text{PdO}_2\text{Cl}_2$, *Chem. Commun.* **50**, 5915 (2014).
- [101] H. Pausch and H. Müller-Buschbaum, Präparation von SrNiO_2 -einkristallen mit eben koordiniertem nickel, *Z. Anorg. Allg. Chem.* **426**, 184 (1976).
- [102] Y. Takeda, T. Hashino, H. Miyamoto, F. Kanamaru, S. Kume, and M. Koizumi, Synthesis of SrNiO_3 and related compound, $\text{Sr}_2\text{Ni}_2\text{O}_5$, *J. Inorg. Nucl. Chem.* **34**, 1599 (1972).
- [103] H. Kageyama, K. Hayashi, K. Maeda, J. P. Attfield, Z. Hiroi, J. M. Rondinelli, and K. R. Poeppelmeier, Expanding frontiers in materials chemistry and physics with multiple anions, *Nat. Commun.* **9**, 772 (2018).
- [104] E. Dagotto, J. Riera, and D. Scalapino, Superconductivity in ladders and coupled planes, *Phys. Rev. B* **45**, 5744 (1992).
- [105] F. Aryasetiawan, M. Imada, A. Georges, G. Kotliar, S. Biermann, and A. I. Lichtenstein, Frequency-dependent local interactions and low-energy effective models from electronic structure calculations, *Phys. Rev. B* **70**, 195104 (2004).
- [106] M. Kaltak, Merging GW with DMFT, PhD thesis, Universität Wien (2015).